

Rhodamine bound maghemite as a long-term dual imaging nanoprobe of adipose tissue-derived mesenchymal stromal cells

Vratislav Cmiel¹ · Josef Skopalik² · Katerina Polakova³ · Jan Solar⁴ ·
Marketa Havrdova³ · David Milde³ · Ivan Justan^{2,4} · Massimiliano Magro⁵ ·
Zenon Starcuk⁶ · Ivo Provaznik¹

Received: 24 February 2016 / Revised: 25 October 2016 / Accepted: 2 November 2016 / Published online: 26 November 2016
© European Biophysical Societies' Association 2016

Abstract In the last few years, magnetically labeled cells have been intensively explored, and non-invasive cell tracking and magnetic manipulation methods have been tested in preclinical studies focused on cell transplantation. For clinical applications, it is desirable to know the intracellular pathway of nanoparticles, which can predict their biocompatibility with cells and the long-term imaging properties of labeled cells. Here, we quantified labeling efficiency, localization, and fluorescence properties of Rhodamine derivatized superparamagnetic maghemite nanoparticles (SAMN-R) in mesenchymal stromal cells (MSC). We

investigated the stability of SAMN-R in the intracellular space during a long culture (20 days). Analyses were based on advanced confocal microscopy accompanied by atomic absorption spectroscopy (AAS) and magnetic resonance imaging. SAMN-R displayed excellent cellular uptake (24 h of labeling), and no toxicity of SAMN-R labeling was found. 83% of SAMN-R nanoparticles were localized in lysosomes, only 4.8% were found in mitochondria, and no particles were localized in the nucleus. On the basis of the MSC fluorescence measurement every 6 days, we also quantified the continual decrease of SAMN-R fluorescence in the average single MSC during 18 days. An additional set of analyses showed that the intracellular SAMN-R signal decrease was minimally caused by fluorophore degradation or nanoparticles extraction from the cells, main reason is a cell division. The fluorescence of SAMN-R nanoparticles within the cells was detectable minimally for 20 days. These observations indicate that SAMN-R nanoparticles have a potential for application in transplantation medicine.

Electronic supplementary material The online version of this article (doi:10.1007/s00249-016-1187-1) contains supplementary material, which is available to authorized users.

✉ Josef Skopalik
j.skopalik@gmail.com

✉ Katerina Polakova
dr.kacka.polakova@gmail.com

¹ Department of Biomedical Engineering, FEEC, Brno University of Technology, Brno, Czech Republic

² Department of Human Pharmacology and Toxicology, Faculty of Pharmacy, University of Veterinary and Pharmaceutical Sciences, Brno, Czech Republic

³ Regional Centre of Advanced Technologies and Materials, Department of Physical Chemistry, Experimental Physics and Analytical Chemistry, Faculty of Science, Palacky University, Olomouc, Czech Republic

⁴ International Clinical Research Center, St. Anne's University Hospital Brno, Brno, Czech Republic

⁵ Department of Comparative Biomedicine and Food Science, University of Padua, Padua, Italy

⁶ Institute of Scientific Instruments, The Czech Academy of Sciences, Brno, Czech Republic

Keywords Intracellular fluorescent labels · Stem cell tracking · Dual contrast agents · Iron oxide nanoparticles · Confocal microscopy · Mesenchymal stromal cells · Rhodamine

Introduction

Nanoparticles are considered to be an emerging tool that could have significant benefit in all branches of medicine and in all sectors of biomedical research and industry. Nanoparticles are tested in the field of therapy (specific drug delivery, photothermal therapy) and diagnostics (biosensing in vivo, contrast agent for magnetic resonance imaging, stem cell tracking, optical imaging). They are also used in

in vitro assays (magnetic cell separation, transfection, protein and enzyme immobilization), and across-the-board in cancer research (Medeiros et al. 2011; Neoh and Kang 2012; Shinkai 2002; Skopalik et al. 2014; Figuerola et al. 2010). In the field of medicine, the labeling of cells with nanoparticles is a relatively new application. Compared to microparticles, nanoparticles (with a diameter of less than 100 nm) have a significantly greater uptake by cells and the major factors in cell uptake process are given by surface characteristics (polymer coating, surface charge, specific ligands or aptamers) (Desai et al. 1997; Verma et al. 2010; Kobayashi et al. 2014). The intracellular labeling methods are tested especially for cells usable in transplantation programmes (bone marrow cells, mesenchymal stromal cells, immunomodulatory cells) (Medeiros et al. 2011; Skopalik et al. 2014; Figuerola et al. 2010; Ahrens et al. 2003; Daldrup-Link et al. 2003; Lewin et al. 2000). Magnetic ferumoxides nanoparticles (commonly superparamagnetic, thus suitable for MRI), and carbon-based nanoparticles (with fluorescent properties) are mostly used for these intracellular labeling (Zhang et al. 2009; Bernsen et al. 2015; Havrdova et al. 2016).

Nanoparticles with “dual contrast” or “dual signal” ability (e.g. with possibility of fluorescence detection and parallel detection by MRI) form a small subgroup from all intracellular nanolabels in the literature; however, their special properties arouse great expectation (Neoh and Kang 2012; Lai et al. 2012; Souza et al. 2013).

A very few of these “dual signal/contrast nanoparticles” described in the literature underwent precise microscopical evaluation in terms of quantification of nanoparticle uptake by a single cell, precise quantification of nanoparticle mass in cytoplasm and internal organelles, and quantification of retention and degradation in the cells during hours and days after labeling. This precise evaluation needs high-tech instrumentation with submicrometer spatial resolution, like confocal microscopy, and also spectroscopic instrumentation, analytical chemistry technique for detection of picogram amount of nanoparticles in small cell samples, accompanied by instrumentation for magnetic resonance imaging. All these analytical methods were recently established and used for testing of modern nanolabels called SAMN-Rhodamine (SAMN-R) at our workplace. In the study described below, we have tested the labeling efficiency, redistribution, localization, and quantification of SAMN-R nanoparticles within subcellular compartments of the stem cells. The total fluorescence of internalized nanoparticles (and its decrease during cell division) has been precisely quantified and correlated with independent chemical analysis of intracellular iron concentration. Our results proved that fluorescence of SAMN-R inside the cells is detectable for more than 2 weeks and nanoparticles displayed very low speed of degradation in the subcellular compartments. These “dual signal/contrast” SAMN-R

show excellent properties for future labeling and tracking of transplanted cells in animal or clinical studies.

Materials and methods

Synthesis and characterization of SAMN-R nanoparticles

The synthesis of SAMN iron oxide nanoparticles has been described before (Magro et al. 2012; Sinigaglia et al. 2012; Venerando et al. 2013). Briefly, 10 g of ferric chloride— $\text{FeCl}_3 \cdot 6\text{H}_2\text{O}$ (37 mmol) dissolved in 800 mL of deionized water was reduced by addition of 2 g of NaBH_4 borohydride (3.5%, 100 mL) at room temperature. The black colored precipitate was then boiled for 2 h at 100 °C, cooled to room temperature, separated by external magnet and washed several times with water. In the final step, the intermediate product was thermally treated at 400 °C for 2 h. The obtained maghemite nanoparticles called SAMN were dispersed in deionized water in ultrasonic bath.

The surface of bare SAMN nanoparticles (100 mg L^{-1}) has been superficially and reversibly functionalized by simple incubation in 50 mM tetramethylammonium perchlorate, pH 7.0, in the presence of 50 μM Rhodamine B isothiocyanate (RITC). The test tube was gently shaken for 1 hour at room temperature. After the incubation period, nanoparticles were separated using an external magnetic field. The amount of bound RITC was calculated from the disappearance of the RITC absorbance at 554 nm in the supernatant (Magro et al. 2012; Venerando et al. 2013). After magnetic separation, SAMN-R particles were washed in 50 mM tetramethylammonium perchlorate to confirm no leaching of the Rhodamine derivate, determined from absorbance spectroscopy of the supernatant. FTIR analysis was used for surface analysis of SAMN nanoparticles.

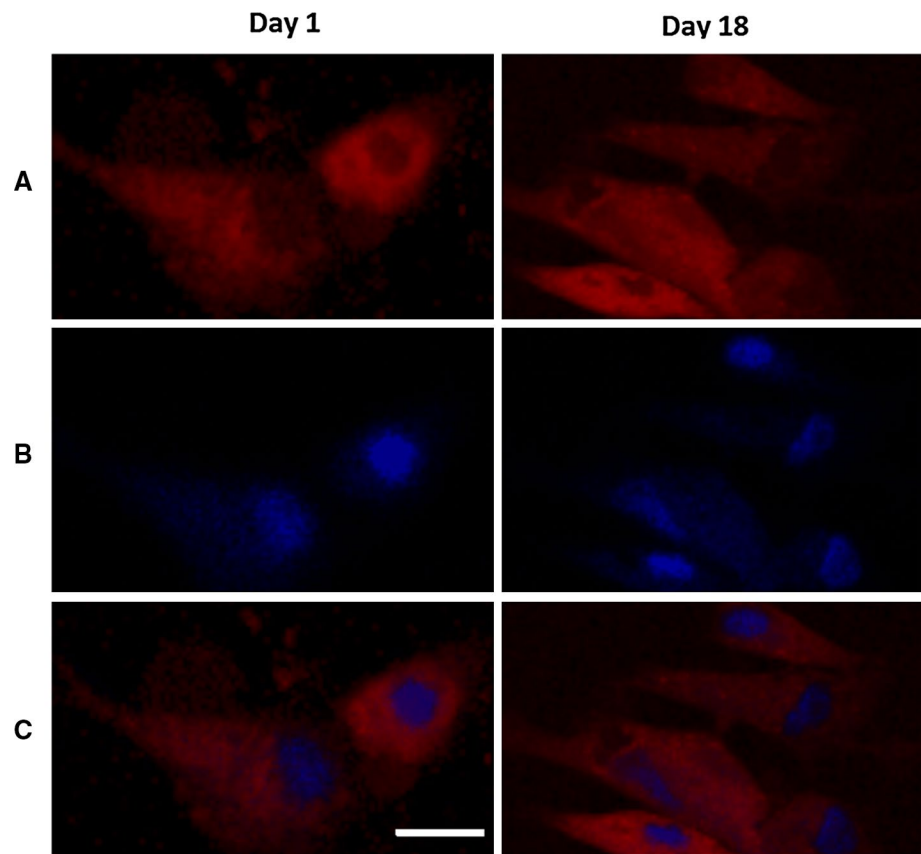
The shape and size of SAMN-R nanoparticles were imaged by two different FE-SEM instruments (JEOL 7401F and Hitachi SU6600), details in (Havrdova et al. 2014).

SAMN-R labeled cell samples were used for demonstration of magnetic/fluorescence signal. Basic test of SAMN-R labeled cells visualization were based on set up of 4.7 T MRI and a digital camera with front orange-red wavelength filters (details in Supplement 1). Additional quantification of MRI contrast of SAMN-R labeled cells in macroscopic fantoms was realized using standard clinical 1.5 T MRI instrumentation (Signa HORIZON Lx, GE Healthcare) (Supplement 1).

Cell cultures preparation and cell labeling by SPIO

Human adipose tissue derived MSCs were isolated from fatty tissue of three healthy donors who had undergone

Fig. 1 Microphotos of MSC cells after SAMN-R incorporation. **a** SAMN-R red fluorescence (filters 520/590), **b** Hoechst fluorescence (filters 405/490 nm), **c** Digital merge of both color frames. Olympus IX-70, objective 10×, *bar* 25 μm



cosmetic liposuction (one male, two females). Isolation of MSCs was based on incubation of lipoaspirates with collagenase. MSCs were expanded in complete Dulbecco's modified Eagle's medium (plus 5% platelet lysate) for 3 weeks (population doublings reached value 7.2–8.5 for the cell samples from different donors). Details of isolation and incubation are described in Supplement 8; typical MSC phenotypes were tested on each culture before start of the nanoparticles experiments (see Supplement 9). All collections of waste lipoaspirates from liposuction were performed after approval of the ethical committee and with informed consent of patients.

The optimal way for incorporation of SPIO nanoparticles into the cells was pre-evaluated in our previous study (Skopalik et al. 2014). The safety labeling concentration was 50 μg per ml of culture medium (24 h incubation time). The continual increase of SAMN-R nanoparticles deposit in the cells during 24 h of labeling can be visualized by standard fluorescence microscopy (Fig. 1).

Basic cytotoxic analysis

Labeled MSCs were trypsinized and seeded at density $2.5 \times 10^3/\text{cm}^2$ in a culture dish (type D35-14-1.5-N, InVitro Scientific, coated by poly-D-lysine). The culture medium [Dulbecco's modified Eagle's medium, Sigma-Adrich; was

supplemented with 100 U/mL of penicillin/streptomycin (GIBCO Biosciences) and 5% platelet lysate; details in Supplement 8]. The medium was exchanged every 3 days. Standard morphology, viability, and CD markers of MSCs were checked before and after SAMN-R labeling and during next 18 days:

- Viable cells in culture chamber were quantified each 6 days using a Calcein—EtHD viability kit (Invitrogen) and Olympus IX 70 epifluorescence microscope.
- Markers CD90, CD73, CD105, and CD34 expression using FACS (BD FACSCanto, BD Biosciences) were quantified; methodology and results are described in Supplement 9.
- Test of unaffected osteogenic, adipogenic, and chondrogenic potential of cells after SAMN-R labeling was prepared with the use of Osteogenesis Differentiation Kit (Invitrogen), Adipogenesis Differentiation Kit (Invitrogen), Chondrogenesis Differentiation Kit (Invitrogen); details and results in Supplement 9.

Cell cultures from three donors underwent also additional special test under hypoxic conditions. SAMN-R labeled cells were seeded at a density of $2.5 \times 10^3/\text{cm}^2$ and put to hypoxic incubator (HeraCell 150i, ThermoFischer Scientific; 5% O_2). Viability and phenotype were quantified in the next 18 days by the same methods used for normoxic cells.

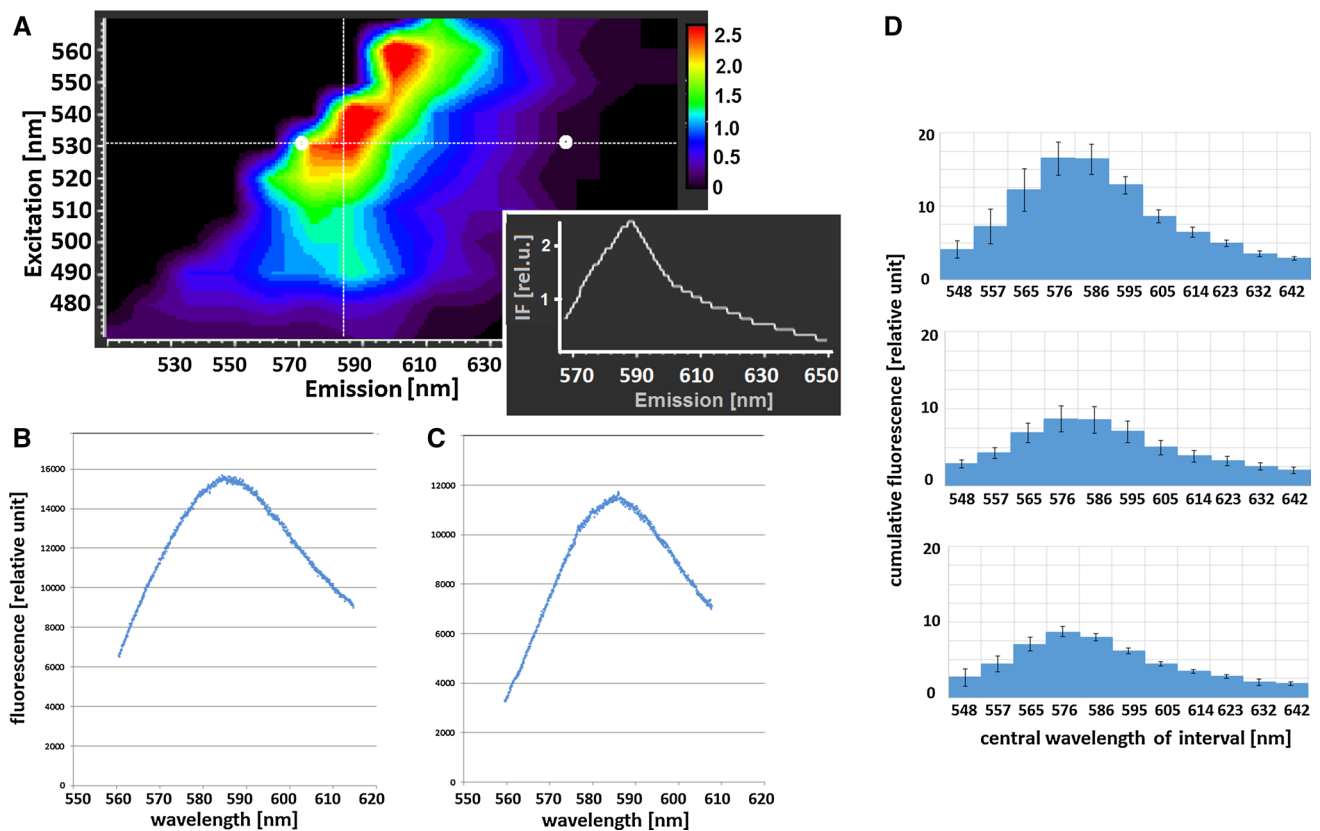


Fig. 2 **a** Results of Lambda scan (excitation/emission spectrum) for the typical cell after 24 h SAMN-R labeling. Laser 530 nm induces a “wide peak” of emission with a maximum at 580 nm. Spectroscopic measurement of **(b)** free SAMN-R (not incorporated in the cells) diluted in physiological solution, **c** SAMN-R incorporated in the cells, which were resuspended in the physiological solution. The

main peaks are comparable with published spectra of free Rhodamine (Zehentbauer et al. 2014). **d** Spectral properties of SAMN-R labeled cells during 18 days. Fluorescence intensity was measured for each 15 nm wide interval (numbers on the horizontal axis represent a center of interval), from the top: day 1, 12, 18

Confocal microscopy: basic characterization of SAMN-R fluorescence by 2D spectral analysis

Unlabeled MSC (control cells) were trypsinized and seeded to microscopic chamber (type D35-14-1.5-N, InVitro Scientific, D35-14-1.5-N, InVitro Scientific, coated by poly-D-lysine). MSC labeled by SAMN-R nanoparticles were re-seeded in the same way. The fluorescence properties of control MSC and MSC labeled by SAMN-R particles were determined using “XYλ Lambda Scan Function” integrated in confocal microscope Leica TCS SP8X (objective 10×). Scan of each MSC was maintained in one optimal z -position (the horizontal plane in half distance between bottom and top of the cell body). Two-dimensional spectral lambda scan with a help of tunable White Light Laser (WLL) and extra-sensitive hybride detectors (HyD) enable analysis of the fluorescence emission or excitation-emission spectral properties. Excitation interval was set from 540 to 650 nm and emission interval from 550 to 800 nm with a scanning

band of 15 nm width and step 15 nm. The two-dimensional spectrum was collected from each of 50 randomly selected MSC and visualized by Leica LAS X software (visualization for one representative MSC on Fig. 2a).

Characterization of stability of SAMN-R fluorescence spectrum by 1D spectral analysis, quantification of total signal and ferumoxide content in one MSC

After two-dimensional spectral analysis, each MSC sample was placed into the sample holder of a confocal microscope, the scanning mode was reconfigured to one-dimensional “XYλ Lambda Scan” and applied to MSC sample (the excitation was fixed at 530 nm; the interval of detection was 540–750 nm). The 1D spectral scanning protocol was applied at day 1 and repeated every 6 days; the spectral scans were derived from 10 randomly selected single MSC bodies, and average 1D spectral histogram was constructed (Fig. 1d).

After the verification, which shows that emission spectrum of SAMN-R labeled MSC has a relatively stable shape in the range from 550 to 700 nm during the 18 days, detection interval of Leica TCS SP8X was fixed to 550–700 nm, and this detection window in combination with laser excitation 530 nm was used for advanced quantitative measurement of total fluorescence intensity of labeled MSC: fluorescence scans were taken from N horizontal planes inside the cell (parallel to the central plane, which was described above), z -positions were commonly in a total interval of 0–30 μm (maximally 0–50 μm), stepsize 4.5 μm (commonly $N = 30 \mu\text{m}/4.5 \mu\text{m}$). Three-dimensional reconstruction and projection of Z-stacks was performed with the Leica LAS X software; MATLAB utility enabled us to compute weighted summation of the positive pixels (which have fluorescence intensity above the threshold of background noise) in the volume inside the cells. This summa for one MSC cell is further called as SWBOS (“Summary of whole cell body orange-red fluorescence signal”). The definitions of cell borders and other details of the MATLAB utility are attached in Supplement 3.

SWBOS mean values were computed from 100 single cells immediately after 24 h of labeling and from 100 single cells in different time points (day 3, 6, 12, and 18 after labeling) by the MATLAB utility. Extra samples of 50 cells also underwent the SWBOS computing during labeling process (0, 6, 12, and 18 h of labeling). In all described confocal scanning analyses, the laser was set to minimize photobleaching effect of Rhodamine and risk of phototoxicity (the Leica facial panel elements standardly set to: laser intensity value of 5%, scanning rate value of 100, averaging value of 3, and the bright field scanning was obtained strictly after fluorescence scanning and its duration minimized to 2–5 s). Visual overview of Leica facial panels and summary of scanning parameters are attached in Supplement 4.

Besides “optical” SWBOS quantification at day 0, 6, 12, and 18, SAMN-R nanoparticle’s concentration inside the cells was also characterized by AAS (SAvantAA; GBC—Scientific Equipment, Australia). The MSC from the same time points and culture dish were used. Briefly, each cell sample was trypsinized, quantified by Bürker chamber, and 0.2×10^6 of cells were immediately diluted in the mixture of 100 μl of 65% HNO_3 and 400 μL of water (demineralized water 18.2 $\text{M}\Omega \text{ cm}$). Measurement was repeated in triplicate. External calibration solutions in the range of 0.5–8 mg/L were prepared by diluting a certified reference material—water calibration solution with Fe concentration $1.000 \pm 0.002 \text{ g/L}$ (Analytika, spol. s r.o., Prague, Czech Republic). The μg iron content in cell sample was quantified; pg content per one average cell was computed.

Localization of SAMN-R in subcellular compartments

SAMN-R labeled cells were stained by the specific mitochondrial marker. Several types of commercial markers were tested. Our main criterion for the selection of the best marker was a minimal spectral overlap with SAMN-R “orange” fluorescence and non-affected cell viability (vital staining without fixation). The final selection was CytoPainter Mitochondrial (Abcam). Another freshly SAMN-R labeled cell sample was stained with several fluorescent markers for lysosome. Cell Navigator™ Lysosome Staining Kit—green (AAT Bioquest) was selected as the best marker. Final staining procedure for CytoPainter and Cell Navigator was adopted from datasheet of these commercial kits: adherent cells in confocal microchamber were washed by prewarmed Hanks’ salt solution, surface of chamber (1 cm^2) was covered by 200 μL of prewamed DMEM (glucose 1 g/L), 1 μL of the staining probe solution was mixed with 500 μL of buffer from the staining kit, 20 μL of the final solution was dropped into the microchamber. Cells were kept in the dark within a cell incubator for 20 min, washed, and after the next 20 min cells were scanned by confocal microscope. All the steps were performed under 37 °C.

Cells were scanned by objective 63 \times , the volume of each single cell was divided into 6–10 confocal planes and scanned in two (“orange” and “green”) detection channels (details in Results). All frames from each color channel were exported to tiff—files and the MATLAB software enabled colocalization of “orange” SAMN-R pixels and “green region” of lysosomes (or mitochondria respectively) for each single cell.

Fluorescence properties of Rhodamine in different subcellular microdomains

The excitation-emission 2D spectrum and lifetime of SAMN-R fluorescence in different subdomains of labeled cells and on different days after labeling were also measured by Leica confocal microscope. The reason for this measurement is investigation of hypothetical different degradation of Rhodamine in different parts of cells or over time (degradation could be manifested as a change in a decay curve of fluorescence and/or shift of fluorescent peak). All details are described in Supplement 5.

Statistical analysis

Cell viability, proliferation, physiological function or intracellular fluorescence, and nanoparticle deposit were measured and quantified on statistically relevant cell samples:

- (a) Viability and morphology of control and nanoparticle-treated cells was quantified on 10 wide fields of light microscope (objective 10 \times) for each cell culture (three cultures, each from different donors). Differences of viability between control and treated group at each time point were evaluated by the Wilcoxon test ($p < 0.05$, details in figure legends). Phenotype (CD-markers positivity) was measured on 10³ cells from all control and nanoparticle-treated groups of all three donors; one representative histogram for control and one for treated group was selected.
- (b) 2D “Lambda scans” was conducted on 50 randomly selected cells from each cell culture (three cultures = three donors) after SAMN-R labeling, all results were visualized by 2D heat maps, one the most representative heat map was presented as Fig. 2a. 1D spectral analysis (emission spectrum for fixed excitation 530 nm) was measured for each from three cultures (50 randomly selected cells from each culture was measured at day 1 after nanoparticle treatment, one average spectral histogram from each 50 randomly selected cells was constructed, cross-culture similarity of three spectral histograms were approved by the Pearson’s Chi squared test (p value criterion 0.05), after that one representative histogram from Culture#2 was selected for Fig. 2d, upper image). Analogical histograms and statistics were constructed for day 12 and day 18 (Fig. 2d, lower images).
- (c) Spectral scan of fluorescence life time: 10 cell bodies (minimally three cells from three independent cell cultures, four randomly selected regions of interest in each cell) were measured for each time point. The representative time-decay curve was selected (details in Supplement 5).
- (d) SWBOS quantification: 100 cells were randomly selected from each cell culture (each of three donors) at day 1, 6, 12, and 18; average SWBOS \pm S.D. was computed for each time point and each culture. Average SWBOS values was used time-curve construction, time-curve from one representative culture was used for Fig. 3. after statistical approving of cross-culture similarity of SWBOS (one each culture with other two cultures were compared by two side t test (p value criterion 0.05), three independent tests for each time point).
- (e) AAS quantification: 0.2×10^6 cells were collected from each cell culture at day 1 or day 6, 12, 18, respectively, pg content per 0.2×10^6 cells was measured in triplicate, pg of iron per one average cell was computed and average \pm S.D. for each day and culture was quantified. Time curve for one representative cell culture was used in Fig. 3.
- (f) Statistical significance of differences between relative value of “real measured SWBOS” and relative value of “SWBOS computed from theoretical model of cell division” (red curve versus black curve, Fig. 3c) was approved for set of three cultures by Wilcoxon signed-rank tests (p value criterion 0.05) for each time point >6 days. The differences were also expressed as mean \pm S.D. in extra graph with horizontal time axis (Fig. 3d). The same statistical method was used for difference of “real measured SWBOS” and “AAS” curve (details in Fig. 3d legend).

Results

Physical and chemical characterization of SAMN-R nanoparticles

As mentioned in our previous works (Magro et al. 2012; Sinigaglia et al. 2012), SAMN consists of 10 ± 2 nm globular maghemite nanoparticles. The surface of the particles interacts with surrounding water molecules, thus maintains low inter-particle forces and good colloidal stability. At 300 K, SAMN reveal a very high magnetization of nearly 71 A m²/kg at 7 T, which is comparable to the value for bulk maghemite (85 A m²/kg). The amount of bound Rhodamine was calculated from the disappearance of the Rhodamine absorbance at 554 nm in the supernatant ($\epsilon = 6.6 \times 10^4$ M⁻¹ cm⁻¹). It was shown that fluorescent magnetic nanoparticles were comprised of 29.1 ± 3.8 μ mol Rhodamine per g of SAMNs (Sinigaglia et al. 2012). Rhodamine is able to bind to the nanoparticle’s surface due to the coexistence of isothiocyanate and an amino groups which can anchor the surface of the SAMN (confirmed by FTIR spectroscopy) (Venerando et al. 2013). From microscopy analysis, it was revealed that SAMN-R exhibit a very homogenous population of particles with an average size of 15 nm in physiological saline solution (Skopalik et al. 2014). The zeta potential of the particles in saline solution and in the culture medium was -22.5 mV. MRI phantom tests showed that SAMN and also SAMN-R are efficient MRI contrast agents (Fig. S-1). Comparison of contrast properties with commercial Resovist is attached (Fig. S-1).

Characterization of cell viability

A concentration of 50 μ g/mL of SAMN-R (directly added to cultivation medium without need of any transfection agents) and 24 h of the labeling were found to be sufficient and safe conditions for MSC labeling, similarly to results of (Skopalik et al. 2014). Statistical results are summarized in Supplement 2. There was no statistical difference in

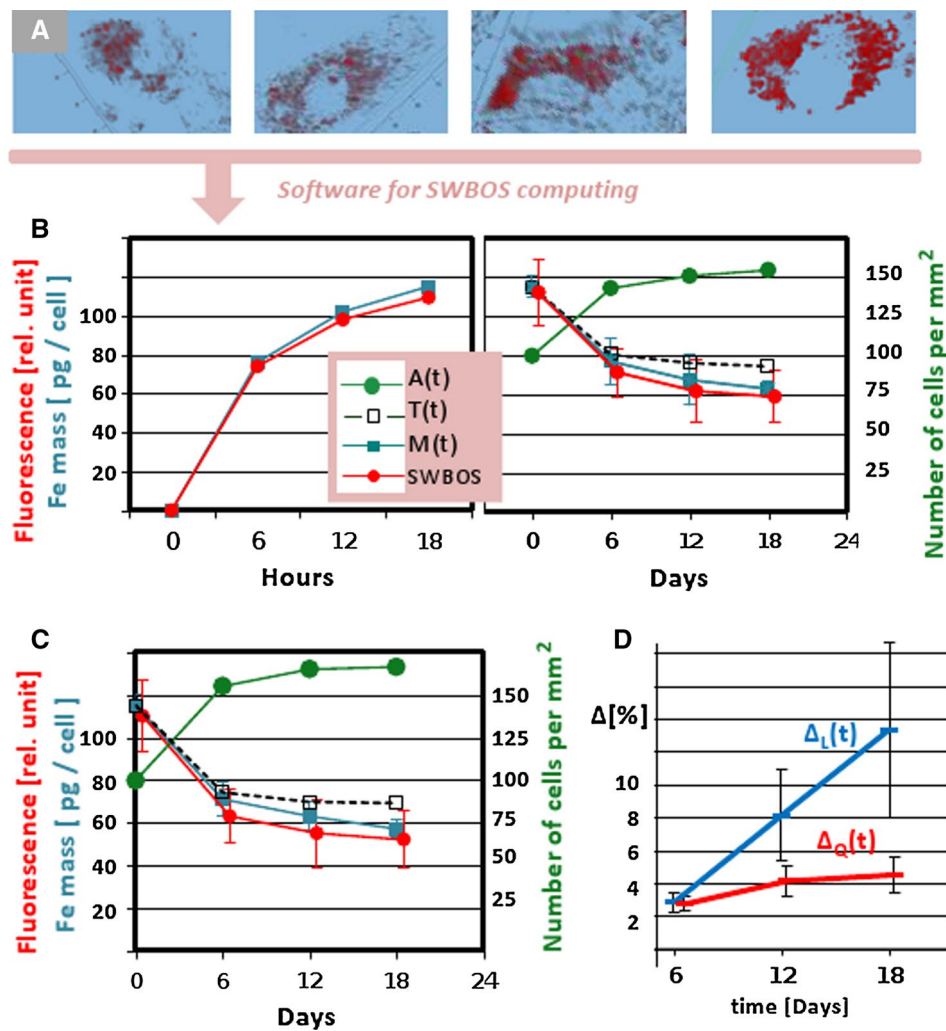


Fig. 3 **a** Example of representative set of MSC microphotographs where the continual SAMN-R fluorescence increase is evident during the time (time-points 6, 12, 18, 24 h after start of the labeling; performed by Leica LAS software). **b** Statistical summary of cell number kinetics within the chamber, SAMN-R deposit and SWBOS kinetics under normoxic condition. A(t) function (green line) = increasing total amount of the cells on 1 mm²; T(t) function (black dot line) = theoretical average mass of iron per cell (constructed as a total iron nanoparticles deposit at the start/actual number of cells in time t); M(t) function (blue line) = real average mass of iron nanoparticles deposit inside one cell, obtained from AAS measurement; SWBOS(t) function (red line) = average intensity of fluorescence per cell (definition in methods), measured by confocal microscope. A reported graph

is the representative result from three analyses (three independent cell samples from three donors). A computing of mean \pm S.D. is described in “Materials and methods”. **c** Statistical summary of cell number kinetics within the chamber, SAMN-R deposit and SWBOS kinetics under hypoxic condition. **d** The average value of “SAMN-R loss per cell” $\Delta_L(t) = 100\% \times [T(t) - M(t)] / T(t)$ derived from three independent cell samples and the average value of “SAMN-R quenching per cell” $\Delta_Q(t) = 100\% \times [M(t) / M(0) - SWBOS(t) / SWBOS(0)] \times T(0) / T(t)$ also derived from three independent cell samples (50 cells in one sample). The significance of $\Delta_L(t)$ and $\Delta_Q(t)$ was approved by Wilcoxon tests (p value criterion 0.05), independent test for each time point $p > 6$ days

viability of labeled cells and control cells in all days (1, 6, 12, and 18); moreover, no value of viability was observed below 90% for SAMN-R labeled cells (Fig. S-2a). The results for hypoxic culture were very similar (Fig S-2a). Both in normoxic and hypoxic culture SAMN-R nanoparticles did not create any visible dangerous precipitate or clots during 18 days of cultivation. Standard spindle shape morphology of cells was also not affected during the labeling and next 18 days (Fig. 1). Intracellular space was visible

under fluorescence microscope as homogenous “orange-red” area (Fig. 1). The average horizontal projection of the cells after SAMN-R labeling was $1056 \pm 249 \mu\text{m}^2$ for control and $976 \pm 260 \mu\text{m}^2$ for labeled cells (difference is not statistically significant). MSC with internalized SAMN-R showed osteogenic, adipogenic, and chondrogenic differentiation (Supplement 9).

These all aspects of SAMN-R nanoparticles were well comparable with previous generation of SAMN

nanoparticles (Skopalik et al. 2014), and thus biocompatibility and non-toxicity of SAMN-R for MSC were approved.

Confocal microscopy, basic characterization of SAMN-R fluorescence, 2D and 1D spectra

Results of 2D spectral analysis of SAMN-labeled MSC cells are shown in Fig. 2a (result from “XYΛλ Lambda scan” of Leica TCS confocal microscope). The main peak of the fluorescence emission spectra is in the orange-red wavelength. Fluorescent 1D spectra (excitation 530 nm) of SAMN-R were measured additionally also on the macroscopic samples by using Unicam UV 550 spectrophotometer. Figure 2c displays spectrum of SAMN-R, which were incorporated in 5×10^3 cells (resuspended in 1 mL of physiological solution), the shape of the spectrum is very similar to the curves obtained from Leica microscope in Fig. 2a. The spectrum of SAMN-R water solution without cells (50 µg of nanoparticles resuspended in 1 mL of physiological solution) is quantified in Fig. 2b.

Characterization of stability of SAMN-R fluorescence spectrum by 1D spectral analysis, quantification of total signal, and ferumoxide content in one MSC

Spectral analysis on a Leica TCS SP8X confocal fluorescence microscope was performed during 18 days after cell labeling (excitation laser line 530 nm). The comparison of three histograms (Fig. 2d) from different culture time points shows stability of fluorescence maximum near 580 nm and relatively stable shape of fluorescence peak in 550–750 nm interval, without any secondary peak developed during the time of MSC culturing. This evaluation of spectral stability is a very important marker for setting of future quantitative detection system for tracking of transplanted cells (nanoparticles will be visible); detectors should be simply set to the “orange-red” 550–750 wavelength or central main peak.

Cells at the time 0, 6, 12, and 24 h of labeling and on day 6, 12, 18 after SAMN-R labeling were trypsinized and concentrated in the plastic vials by centrifugation (illustration in Fig. 3a). The continual changes of total fluorescence yield per single cells are visible from confocal snapshots obtained during first 24 h and next 18 days. The long-time kinetics of this fluorescence intensity per cell (SWBOS value) and average nanoparticle-ferumoxide content per cell was visualized (Fig. 3b). Both these parameters of cells are decreasing in time and display very significant inverse correlation with the amount of cells in culture (change of the number of cells caused by cell division kinetics; green line in Fig. 3b; details in Discussion).

The same methods of growth curve detection and SWBOS measurement were additionally also repeated for

hypoxic cells (Fig. 3c); results from normoxic and hypoxic culture are compared in “Discussion”.

Localization of SAMN-R in subcellular compartments

The comparison of the excitation/emission spectra of Cytosainter Mitochondrial (Fig. 4a) and SAMN-R implicated possibility of their parallel detection in one sample, the setup 490/500–530 and 570/620–720 nm display sufficient segregation of fluorescence peaks. Typical microphotos of mitochondrial and SAMN-R bodies are reprinted in Fig. 4c. Statistics on confocal frames have shown that only $4.8 \pm 1.2\%$ of “orange-red” pixels (SAMN-R) were located in “green” areas (mitochondria).

The comparison of excitation/emission spectra of Cell Navigator (Fig. 4b) and SAMN-R implicated also possibility of their parallel detection in one sample, final optimized setup 490/500–530 and 570/620–720 nm was used (separated scanning in time, using the “Sequential scan” of Leica control software). $83 \pm 7\%$ of “orange-red” pixels (SAMN-R) had incidence with “green” pixels area (lysosomes). High colocalization of “orange-red” and “green” pixels is evident also from all confocal scans of the cells (example Fig. 4d).

Discussion

Visualization of transplanted cells can expand the horizons of cell therapy. SPIO probes inside the cells detected by magnetic resonance enable unequalled possibility of non-invasive, sensitive, safe, and daily repeatable visualization of transplanted cells in the human or animal body, but the resolution of single cells or subcellular entities is problematic. On the other hand, fluorescence probe in the cells and optical noninvasive detection can be used for very precise localization and quantification of transplanted cells in a shallow location in living soft tissues (epithelium, wall of vessels) or in biopsies or postmortem histological samples, but the long time stability of fluorescence probe is questionable. Modern probes, which combine the advantages of both of these types, can partially eliminate some of their specific limitation and bring novel more precise detection ability (Neoh and Kang 2012; Lai et al. 2012; Souza et al. 2013).

The most common contrast agents for tracking of stem cells by MRI are still ferumoxide nanoparticles. The unaffected viability of cells after nanoparticle uptake is the first important marker, which should be precisely characterized (Medeiros et al. 2011; Neoh and Kang 2012). The amount of intracellular accumulation of nanoparticles after several hours of labeling reaches usually 10–100 pg of ferumoxides per cell (Neoh and Kang 2012; Shinkai 2002; Skopalik

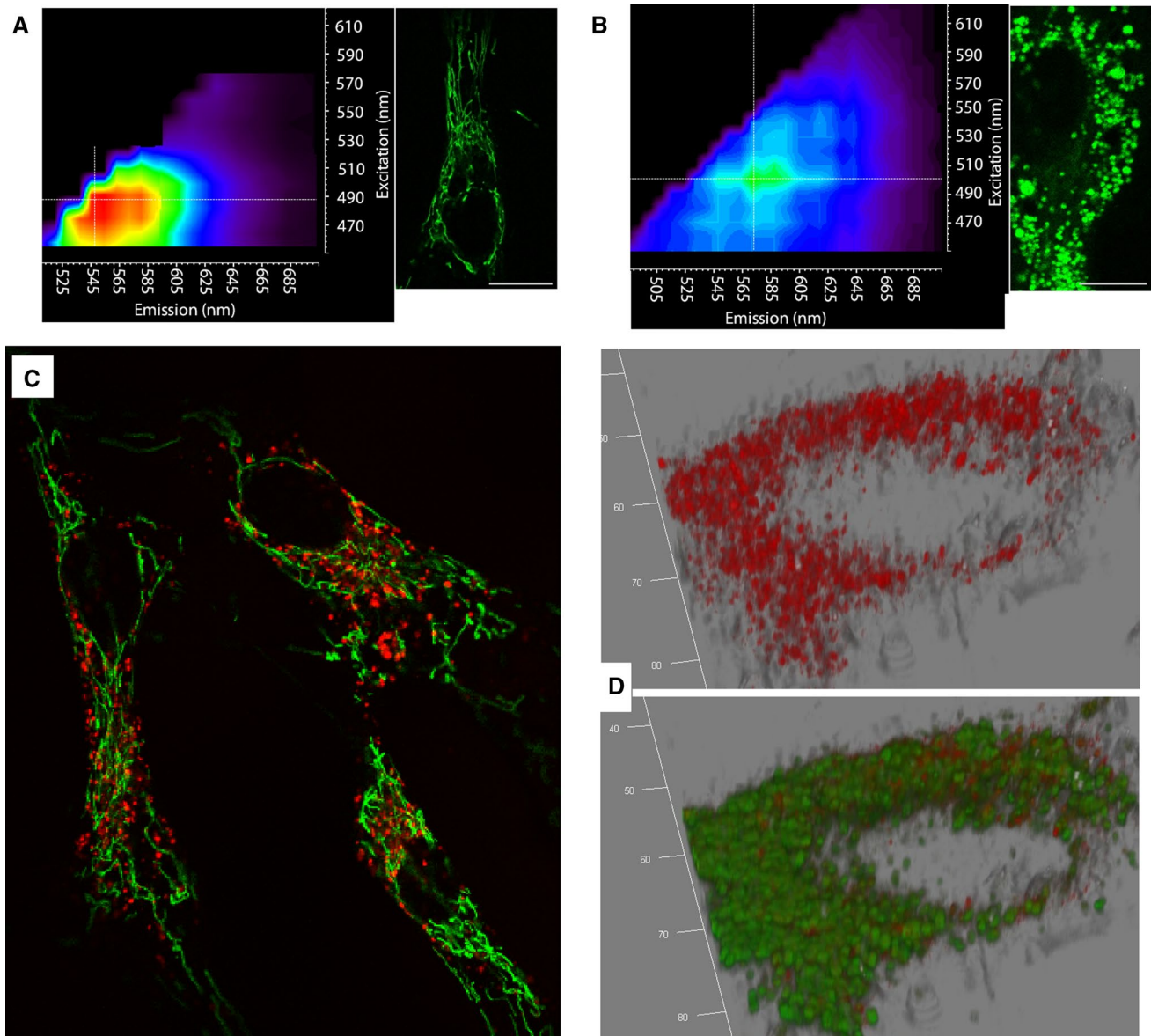


Fig. 4 Excitation/emission spectra of Cytopainter Mitochondrial (a) and Cell Navigator (b), windows on the right side as illustrative confocal scan of labeled cell; objective 63 \times , bar 20 μ m. c Colocalisation analysis of SAMN-R clusters (red pixels) and mitochondria

(green pixels). d Highly evident colocalisation of SAMN-R clusters (red pixels) and lysosomes (green pixels) in one typical MSC. Central “empty circle” is position of nucleus. 3D reconstruction by Leica LAS X software

et al. 2014). Unfortunately, several picograms of some types of nanoparticles have shown insufficient biocompatibility in labeled cells, and their adoption to the practical medicine is problematic or impossible (Kostura et al. 2004; Chang et al. 2012).

In this work, we described intracellular uptake and distribution of novel SAMN-R labels, which consist of superparamagnetic core and fluorescent Rhodamine molecules bound to the surface of the core.

The total mass of SAMN-R accumulated after 24 h of labeling (115 ± 19 pg/cell) is comparable with our

previous experiments on naked SAMN nonconjugated with Rhodamine (Skopalik et al. 2014).

The spindle shape morphology of MSC was not affected after SAMN-R labeling, the 18-days proliferation and viability of SAMN-R labeled cells were not different from results measured on control cells (Supplement 2a). For better mimicking of MSC metabolism after transplantation into the real ischemic tissue we also used hypoxic incubator (5% O₂). These hypoxic cells showed small increase in proliferation rate (10% at day 6; 8% at day 12) against normoxic cells. Our toxicological results on hypoxic cells

are promising contrary to the results of Rosenberg et al. (2013) where iron oxide nanoparticles in hypoxic conditions caused higher cytotoxicity.

Distribution of SAMN-R in lysosomes is similar to published results from older Ferucarbotran studies (Yang et al. 2011). Moreover, the absence of nanoparticles in the nucleus and very minimal incidence in mitochondria confirm SAMN-R biocompatibility in comparison to other studies of nanoprobe (Khan et al. 2012; Derfus et al. 2004). The rest of 10% of SAMN-R red pixels showed no colocalization with lysosomes, mitochondria or nucleus. The topography of these pixels on confocal scans let us to hypothesize that the resting SAMN-R nanoparticles could occur in the early endosomes and/or they could be localized in the area of the cell membrane; however, precise colocalization would be the aim of further analysis. Moreover, SAMN-R labeled stem cells were proved to have unaffected potential to adipogenic, osteogenic, and chondrogenic differentiation (Supplement 9). All above-mentioned cytotoxic results are important for potential utilization of the SAMN-R labeled cells in pre-clinical studies or clinical practice.

Our results from the set of multi-analysis experiments (Fig. 3, where the kinetics of cell population, the kinetics of fluorescence intensity of nanoparticles per cell and kinetics of mass of nanoparticles per cell are combined into one picture) indicate that the total decrease of SAMN-R fluorescence during the time of 18 days [in the mathematical form $\Delta_{\text{TOTAL}}(t) = \text{SWBOS}(0) - \text{SWBOS}(t)$, more details in Fig. 3 legend] is mainly caused by cell division. This total decrease could be ideally described in the mathematical form as $\Delta_{\text{TOTAL}}(t) = \text{SWBOS}(0) \times 0.5^n$, where n is the theoretical number of cell generations derived from each initial cell in culture during the time t (important presumption for using of n and this simple exponential form is a symmetric and synchronous dividing of all cells in culture). This decrease could also be characterized by more practical mathematical form for nonsynchronous cell culture: $\text{SWBOS}(t) = \text{SWBOS}(0) \times \text{initial number of cells/actual number of cells}$. Similar decrease of some type nanoparticles or labels within the cells was observed in many works (Rosenberg et al. 2013; Huang et al. 2013), the phenomenon is called “dilution effect of intracellular labels”. However, Fig. 3 brings the evidence that the real dilution and decrease of SAMN-R deposit is not ideally determined only by the decreasing number of cells, real SWBOS decrease is modulated by two more external factors: “the loss of nanoparticles from the cell” and “quenching (degradation) of Rhodamine”. The loss of the SAMN-R nanoparticle from the cell is possible to quantify exactly from the difference between $M(t)$ and $T(t)$ value [the difference

of the real SAMN-R mass in cell (blue line) and theoretical SAMN-R mass curve (black line)]; this loss of total SAMN-R mass from cells is very low, only ~10% after 12 days (summary from three samples depicts Fig. 3d). Quenching (degradation) of Rhodamine can be quantified as the difference between the value of SWBOS(t) fluorescence intensity (red line) and $M(t)$ ferumoxide mass curve (blue line) in Fig. 3b; the quenching was less than 5% in the 18 days-long observation (details and mathematical description in Fig. 3d).

It is also important to note well-known fact about acidic pH in lysosomes and its degradative effect to many fluorescent probes or nanoparticles, thus, the stability of SAMN-R itself and stability of the bound “Rhodamine—SAMN” were questionable at the beginning of our work. However, our set of complex confocal analysis and AAS analysis approved that (1) the Rhodamine was not dissociated (experiments focused on a decay curve of fluorescence, Fig. S-5) and (2) Rhodamine quenching caused by metabolism of the cell is very low during 18 days after labeling (experiments describing the relatively stable ratio of iron mass and fluorescent intensity of one cell, Fig. 3). Moreover, the stability of the bound “Rhodamine—SAMN” was approved also in our previous paper (Sinigaglia et al. 2012), where the acidic range of pH was tested, too.

Ideal intracellular nanoprobe should have zero “loss of nanoparticles from the cell” and zero “quenching (degradation) of fluorophore”, we proved that SAMN-R display a very low “loss and quenching” phenomena. Moreover, the very low “loss and quenching” phenomena of SAMN-R signal and the validity of correlation between SWBOS(t) and $A(t)$ (cell numbers) was approved also for hypoxic culture (Fig. 3c), the graphs of hypoxic culture show some small acceleration of cell growth in comparison to normoxic cells, and accelerated dilution of SAMN-R. “Loss of nanoparticles from the cell” should be also tested and quantified on MSC culture on special surfaces (different surface chemistry, elasticity, fibrous non-planar structure) in future. These culture condition (Owens et al. 2016, Park et al. 2014 and others) can activate some metabolic pathway and the whole metabolism of cells.

Important questions arise in the literature regarding the contrast properties of the nanoparticles after transplantation of MSC cells into a real tissue, especially for cells with stopped or minimal proliferation. Simulation of this restriction of the proliferation was conducted in one of our additional experiments (details in Supplement 7) where the SAMN-R labeled MSC were seeded with a high confluence and the proliferation was thus minimal. Results showed that the quenching of fluorescence signal or loss of nanoparticle under these conditions are again very low.

Conclusions

The presented new intracellular dual contrast agent SAMN-R is one of the first which underwent precise microscopic evaluation and mathematical description focused on quantification of nanoparticle uptake, quantification of nanoparticle mass in intracellular space and in different internal organelles and correlation of nanoparticle mass (pg/cell) with fluorescence signal during a long-time cell cultivation and cell division. Intracellular stability of the SAMN-R is very high, the continual decrease of signal per one average cell during several weeks can be described by mathematical formula of “dilution effect” in combination with additional empirical corrections (coefficients of “nanoparticles loss” and “Rhodamine quenching” during the time). Results of this in vitro study are important and necessary for following advanced investigation of SAMN-R retention, elimination or degradation in vivo and for safety application of this nano-device in medicine.

Acknowledgements The authors acknowledge the support by Ministry of Education, Youth and Sports of the Czech Republic (project LO1305), the Operational Program “Education for Competitiveness – European Social Fund” CZ.1.07/2.3.00/20.0155. This work was also supported by the project no. LQ1605 from the National Program of Sustainability II (MEYS CR) and by the project FNUSA-ICRC no. CZ.1.05/1.1.00/02.0123 (OP VaVpI). Support by Ministry of Education of the Czech Republic (LO1212 and LO1305, CZ.1.05/2.1.00/01.0017) and the support by Student Project IGAPrF-2015017 is also acknowledged.

References

- Ahrens ET, Feili-Hariri M, Xu H et al (2003) Receptor-mediated endocytosis of iron oxide nanoparticles provides efficient labeling of dendritic cells for in vivo Mr imaging. *Magn Reson Med* 49:1006–1013
- Bernsen MR, Guenoun JG, Van Tiel ST, Krestin GP (2015) Nanoparticles and clinically applicable cell tracking. *Brit J Radiol* 88:20150375
- Chang ZK, Liu ZP, Ho JH et al (2012) Amine-surface-modified superparamagnetic iron oxide nanoparticles interfere with differentiation of human mesenchymal stem cells. *J Orthop Res* 30:1499–1506
- da Rocha EL, Caramori GF, Rambo CR (2013) Nanoparticle translocation through a lipid bilayer tuned by surface chemistry. *Phys Chem Chem Phys* 15:2282–2290
- Daldrup-Link HE, Rudelius M, Oostendorp RA et al (2003) Targeting of hematopoietic progenitor cells with MR contrast agents. *Radiology* 228:760–767
- Derfus AM, Chan WCW, Bhatia SN et al (2004) Intracellular delivery of quantum dots for live cell labeling and organelle tracking. *Adv Mater* 16:961–966
- Desai MP, Labhasetwar V, Walter E et al (1997) The mechanism of uptake of biodegradable microparticles in Caco-2 cells is size dependent. *Pharm Res* 14:1568–1573
- Farrell E, Wiewolski P, Pavljasevic P (2008) Effects of iron oxide incorporation for long term cell tracking on MSC differentiation in vitro and in vivo. *Biochem Biophys Res Commun* 369:1076–1081
- Figuerola A, Di Corato R, Manna L et al (2010) From iron oxide nanoparticles towards advanced iron-based inorganic materials designed for biomedical applications. *Pharmacol Res* 62:126–143
- Havrdova M, Polakova K, Skopalik J et al (2014) Field emission scanning electron microscopy (FE-SEM) as an approach for nanoparticle detection inside cells. *Micron* 67:149–154
- Havrdova M, Hola K, Skopalik J et al (2016) Toxicity of carbon dots—effect of surface functionalization on the cell viability, reactive oxygen species generation and cell cycle. *Carbon* 99:238–248
- Huang X, Zhang F, Wang H, Niu G, Choi KY, Swierczewska M (2013) Mesenchymal stem cell-based cell engineering with multifunctional mesoporous silica nanoparticles for tumor delivery. *Biomaterials* 34(7):1772–1780
- Huang ZY, Li CG, Yang S (2015) Magnetic resonance hypointensive signal primarily originates from extracellular iron particles in the long-term tracking of mesenchymal stem cells transplanted in the infarcted myocardium. *Int J Nanomed* 10:1679–1690
- Khan MI, Mohammad A, Patil G et al (2012) Induction of ROS, mitochondrial damage and autophagy in lung epithelial cancer cells by iron oxide nanoparticles. *Biomaterials* 33:1477–1488
- Kobayashi K, Wei J, Iida R et al (2014) Surface engineering of nanoparticles for therapeutic applications. *Polym J* 46:460–468
- Kostura L, Kraitchman DL, Mackay AM et al (2004) Feridex labeling of mesenchymal stem cells inhibits chondrogenesis but not adipogenesis or osteogenesis. *NMR Biomed* 17:513–517
- Lai SM, Tsai TZ, Hsu CY et al (2012) Bifunctional silica-coated superparamagnetic FePt nanoparticles for fluorescence/MR dual imaging. *J Nanomater* (2012) Art No 631584
- Lewin M, Carlesso N, Tung CH et al (2000) Tat peptide-derivatized magnetic nanoparticles allow in vivo tracking and recovery of progenitor cells. *Nat Biotechnol* 18:410–414
- Magro M, Sinigaglia G, Nodari L et al (2012) Charge binding of rhodamine derivative to OH- stabilized nanomagnhemite: universal nanocarrier for construction of magnetofluorescent biosensors. *Acta Biomater* 8:2068–2076
- Medeiros SF, Santos AM, Fessi H, Elaissari A (2011) Stimuli-responsive magnetic particles for biomedical applications. *Int J Pharmaceut* 403:139–161
- Neoh KG, Kang ET (2012) Surface modification of magnetic nanoparticles for stem cell labelling. *Soft Matter* 8:2057–2069
- Owens GJ, Rajendra KS, Farzad F, Mustafa A (2016) Sol-gel based materials for biomedical applications. *Prog Mater Sci* 77:1–79
- Park J, Park S, Ryu S (2014) Graphene-regulated cardiomyogenic differentiation process of mesenchymal stem cells by enhancing the expression of extracellular matrix proteins and cell signaling molecules. *Adv Healthc Mater* 3(2):176–181
- Rosenberg JT, Sellgren KL, Sachi-Kocher A, Bejarano FC, Baird MA (2013) Magnetic resonance contrast and biological effects of intracellular superparamagnetic iron oxides on human mesenchymal stem cells with long-term culture and hypoxic exposure. *Cytotherapy* 15(3):307–322
- Sen T, Sadhu S, Patra A (2007) Surface energy transfer from rhodamine 6G to gold nanoparticles: a spectroscopic ruler. *Appl Phys Lett* 91:43–104
- Shinkai M (2002) Functional magnetic particles for medical application. *J Biosci Bioeng* 94:606–613
- Sinigaglia G, Magro M, Miotto G et al (2012) Catalytically active bovine serum amine oxidase bound to fluorescent and magnetically drivable nanoparticles. *Int J Nanomed* 7:2249–2259
- Skopalik J, Polakova K, Havrdova M et al (2014) Mesenchymal stromal cell labeling by new uncoated superparamagnetic maghemite

- nanoparticles in comparison with commercial Resovist—an initial in vitro study. *Int J Nanomed* 9:5355–5372
- Souza CGS, Beck W Jr, Varanda LC (2013) Multifunctional lumino-magnetic FePt@ Fe₃O₄/SiO₂/Rhodamine B/SiO₂ nanoparticles with high magnetic emanation for biomedical applications. *J Nanopart Res* 15 Art No 1545
- Stark WJ (2011) Nanoparticles in biological systems. *Angew Chem Int Edit* 50:1242–1258
- Venerando R, Miotto G, Magro M et al (2013) Magnetic nanoparticles with covalently bound self-assembled protein corona for advanced biomedical applications. *J Phys Chem C* 117:20320–20331
- Verma A, Stellacci F et al (2010) Effect of surface properties on nanoparticle-cell interactions. *Small* 6:12–21
- Yang C-Y, Hsiao J-K, Tai M-F et al (2011) Direct labeling of hMSC with SPIO: the long-term influence on toxicity, chondrogenic differentiation capacity, and intracellular distribution. *Mol Imaging Biol* 13:443–451
- Zehentbauer FM, Moretto C, Stephen R et al (2014) Fluorescence spectroscopy of Rhodamine 6G: concentration and solvent effects. *Spectrochim Acta A Mol Biomol Spectrosc* 121:147–151
- Zhang Z, Mascheri N, Dharmakumar R et al (2009) Superparamagnetic iron oxide nanoparticle-labeled cells as an effective vehicle for tracking the GFP gene marker using magnetic resonance imaging. *Cytotherapy* 11:43–51